Travis B. McMurphy,[1,2] Wei Huang,[1,2] Run Xiao,[1,2] Xianglan Liu,[1,2]
Nikhil V. Dhurandhar,[3] and Lei Cao[1,2]

Hepatic Expression of Adenovirus 36 E4ORF1 Improves Glycemic Control and Promotes Glucose Metabolism Through AKT Activation

Diabetes 2017;66:358–371 | DOI: 10.2337/db16-0876

Considering that impaired proximal insulin signaling is linked with diabetes, approaches that enhance glucose disposal independent of insulin signaling are attractive. In vitro data indicate that the E4ORF1 peptide derived from human adenovirus 36 (Ad36) interacts with cells from adipose tissue, skeletal muscle, and liver to enhance glucose disposal, independent of proximal insulin signaling. Adipocyte-specific expression of Ad36E4ORF1 improves hyperglycemia in mice. To determine the hepatic interaction of Ad36E4ORF1 in enhancing glycemic control, we expressed E4ORF1 of Ad36 or Ad5 or fluorescent tag alone by using recombinant adeno-associated viral vector in the liver of three mouse models. In *db/db* or diet-induced obesity (DIO) mice, hepatic expression of Ad36E4ORF1 but not Ad5E4ORF1 robustly improved glycemic control. In normoglycemic wild-type mice, hepatic expression of Ad36E4ORF1 lowered nonfasting blood glucose at a high dose of expression. Of note, Ad36E4ORF1 significantly reduced insulin levels in *db/db* and DIO mice. The improvement in glycemic control was observed without stimulation of the proximal insulin signaling pathway. Collectively, these data indicate that Ad36E4ORF1 is not a typical sensitizer, mimetic, or secretagogue of insulin. Instead, it may have insulin-sparing action, which seems to reduce the need for insulin and, hence, to reduce insulin levels.

Type 2 diabetes often is associated with resistance to insulin signaling, including impaired response of molecular participants of insulin signaling, such as insulin receptor substrate (IRS) 1 or 2 (1–4). This defect in insulin signaling contributes to a reduced response to insulin and a reduced cellular glucose uptake. Most of the currently available antidiabetic medications are sensitizers, mimetics, or secretagogues of insulin, implying their dependence on insulin signaling for optimal benefits. Hence, the class of antidiabetic medications that act independently of IRS-1 or -2 signaling may be more effective and, hence, more-desirable alternatives. To this end, in vitro studies have described E4ORF1, a 125–amino acid peptide derived from human adenovirus 36 (Ad36), that upregulates glucose uptake in adipocytes and their progenitors and myoblasts and reduces glucose release from hepatocytes (5–7). These studies have further indicated that E4ORF1 bypasses IRS-1 or -2 signaling yet improves glucose disposal by upregulating the distal insulin signaling pathway that involves phosphatidylinositol 3-kinase (PI3K), AKT, and GLUT4 through Ras activation (8). Collectively, the data have indicated that E4ORF1 is not a sensitizer, mimetic, or secretagogue of insulin but has an insulin-sparing action (8).

Hence, Ad36E4ORF1 is suggested as a novel target to develop antihyperglycemic drugs, particularly in metabolic syndromes often associated with insulin resistance (8). However, a number of questions remain. First, a detailed characterization of the in vivo effects of Ad36E4ORF1 is not yet reported. Ad36E4ORF1 is not an endogenous secretory protein and, therefore, is unlikely to have a receptor on the cell surface for its uptake, highlighting the challenge in delivering this peptide. Second, whether Ad36E4ORF1 will induce the uncontrolled glucose uptake leading to hypoglycemia in vivo is another unanswered

[1]Department of Cancer Biology and Genetics, Ohio State University, Columbus, OH
[2]The Comprehensive Cancer Center, Ohio State University, Columbus, OH
[3]Department of Nutritional Sciences, Texas Tech University, Lubbock, TX
Corresponding author: Lei Cao, lei.cao@osumc.edu.

Received 21 July 2016 and accepted 21 November 2016.

This article contains Supplementary Data online at http://diabetes.diabetesjournals.org/lookup/suppl/doi:10.2337/db16-0876/-/DC1.

T.B.M. and W.H. contributed equally to this work.

question. Third, the potential oncogenic risk associated with Ras induction by Ad36E4ORF1 should be carefully evaluated in vivo. Although Ad36E4ORF1 interacts with adipose tissue, skeletal muscle, and liver to modulate glucose disposal, the interaction of Ad36E4ORF1 with individual tissues involved in systemic glycemic control is unclear. A recent study showed that fat-specific inducible expression of Ad36E4ORF1 improves glycemic control in DIO mice (9).

To study the interaction of Ad36E4ORF1 with liver, we used a novel recombinant adeno-associated viral (rAAV) serotype vector, Rec2, to deliver Ad36E4ORF1 in vivo. Adenovirus 5 (Ad5) E4ORF1 has been shown to bind to MYC in the nucleus to activate glycolytic targets that promote a Warburg-like shift to anaerobic glycolysis that converts glucose into nucleotides for viral replication (10). However, the in vivo effects of Ad5E4ORF1 alone are not known. We also generated rAAV to deliver Ad5E4ORF1 to determine whether the functions of E4ORF1 are shared across various subfamilies of human adenoviruses.

RESEARCH DESIGN AND METHODS

Mice

C57BL/6 mice, 6 weeks of age, were purchased from Charles River Laboratories (Wilmington, MA). Female *db/db* mice in a C57BL/6 background, 5 weeks of age, were purchased from The Jackson Laboratory (Bar Harbor, ME). Male DIO mice, 12 weeks of age, were purchased from The Jackson Laboratory and maintained on a high-fat diet (60% fat, D12492; Research Diets). All mice were housed in a temperature-controlled room (22°C) with a 12-h light/dark cycle and maintained on standard rodent chow (7912; Teklad) with ad libitum access to food and water. All use of animals was approved by and in accordance with the Ohio State University Animal Care and Use Committee.

rAAV Vector Construction and Packaging

Addgene plasmid 38063 was used as the template for Ad5E4ORF1. Ad36E4ORF1 plasmid was used as previously reported (6). Transgenes destabilized yellow fluorescent protein (dsYFP) and Ad5E4ORF1 or Ad36E4ORF1 were inserted into the multiple cloning sites between the chicken β-actin promoter (cytomegalovirus enhancer and chicken β-actin promoter) and the woodchuck posttranscriptional regulatory element sequence in the rAAV plasmid. rAAV serotype Rec2 vectors were packaged and purified as described elsewhere (11).

db/db Mice

Female *db/db* mice, 5 weeks of age, were randomly assigned to receive a dose of 2×10^{10} vector genomes (vg) of Rec2-Ad5E4ORF1 (n = 8), Ad36E4ORF1 (n = 8), dsYFP (n = 4), or AAV buffer (n = 4) through tail vein injection in 50 μL. Body weight and food intake were monitored periodically. Nonfasting blood glucose was monitored starting 6 days postinjection. A glucose tolerance test (GTT) was performed 3 weeks after AAV injection. Mice were sacrificed 29 days after AAV injection. Trunk blood was collected. Liver and abdominal fat were dissected and weighed. In a separate experiment, *db/db* mice were treated as described above. An insulin tolerance test (ITT) was performed 3 weeks after AAV injection.

DIO Mice

Male DIO mice, 12 weeks of age, were randomly assigned to receive a dose of 2×10^{10} vg of Rec2-Ad5E4ORF1 (n = 8), Ad36E4ORF1 (n = 9), or dsYFP (n = 8) as described above and were maintained on a high-fat diet. GTT was performed 3 weeks post-AAV injection. Body weight, food intake, and nonfasting blood glucose levels were monitored periodically. Mice were sacrificed 7 weeks post-AAV injection.

Wild-Type Mice

Female C57BL/6 mice, 6 weeks of age, were randomly assigned to five groups to receive tail vein injections of rAAV vectors (n = 5 per group) at two doses: Rec2-dsYFP, 2×10^9 vg; Rec2-Ad5E4ORF1, 2×10^9 and 2×10^{10} vg; and Rec2-Ad36E4ORF1, 2×10^9 and 2×10^{10} vg. Nonfasting blood glucose was monitored daily starting 3 days post-rAAV injection. Mice were sacrificed 7 days after rAAV injections.

Perifosine Experiment

Female C57BL/6 mice, 8 weeks of age, were randomly assigned to receive AAV buffer or Rec2-Ad36E4ORF1 (2×10^{10} vg in 50 μL) through tail vein injection. Each vector-injected group was split into two groups to receive perifosine (36 mg per mouse; KareBay BioChem) or PBS by gavage at days 4 and 5 after AAV injection. Nonfasting blood glucose was monitored daily starting on day 4. Mice were sacrificed on day 6 post-AAV injection.

GTT

Mice were injected intraperitoneally with glucose solution (1 mg glucose/g body weight) after an overnight fast. Blood glucose concentrations were measured with a portable glucose meter (CONTOUR NEXT; Bayer).

ITT

Mice were injected intraperitoneally with insulin (0.75 units/kg body weight) at 2:00 P.M. without a fast. Blood glucose levels were measured with a portable glucose meter.

In Vivo Glucose Uptake

Female *db/db* mice, 5 weeks of age, were randomly assigned to receive a dose of 2×10^{10} vg of Ad36E4ORF1 (n = 4) or AAV buffer (n = 4) as described above. The in vivo glucose uptake during a GTT was measured using glucose analog tracer [^{3}H]2-deoxyglucose (2-DG) 8 weeks after rAAV injection by following the published method (12,13). Liver glucose uptake is calculated by dividing [^{3}H] radioactivity in 2-DG-6-phosphate by mean specific activity of glucose during GTT (120 min) and presented as millimole per milligram protein per minute.

Metabolic Parameters

Lipid was extracted from liver by chloroform/methanol (2:1 volume for volume), followed by a rinse in 50 mmol/L NaCl and CaCl (0.36 mol/L)/methanol (1:1 volume for volume) (14). Nonesterified fatty acid, hepatic triglycerides, and

cholesterol quantification were measured using Wako Diagnostics kits. Serum insulin level was determined with mouse insulin ELISA (ALPCO). Serum leptin and adiponectin were measured using a DuoSet ELISA Development System (R&D Systems). Serum glucose was measured with QuantiChrom Glucose Assay kit (DIGL-100). Hepatic glycogen content was measured by hydrolysis of liver tissue in acid followed by colorimetric measurement of the resulting glucose (15). Acetyl-CoA assay was performed with a kit (MAK039; Sigma).

Glucokinase Assay

Fifty milligrams of liver tissue were rinsed with ice-cold PBS and homogenized with a 1.5-mL mortar and pestle in ice-cold PBS containing phosphatase inhibitor and protease inhibitor cocktail. The homogenates were centrifuged and the protein content measured with a BCA Protein Assay Kit (Pierce). The supernatants were immediately subjected to glucokinase (GCK) BioAssay ELISA Kit (United States Biological).

Western Blot

Liver tissues were homogenized in ice-cold radioimmunoprecipitation assay buffer (Pierce) containing 1× PhosSTOP (Sigma) and Protease Inhibitor Cocktail Set III (Calbiochem). Blots were incubated overnight at 4°C with the following primary antibodies: Ad36E4ORF1 (1:1,000; a gift from N.V.D.), GAPDH (1:500, CB1001; Calbiochem), actin (1:3,000, #4970; Cell Signaling), total Ras (1:1,000, #3965; Cell Signaling), c-Myc (1:1,000, #5605; Cell Signaling), phospho-AKT(Ser473) (1:1,000, #9271; Cell Signaling), phospho-AKT (Thr308) (1:1,000, #9275; Cell Signaling), total AKT (1:1,000, #9272; Cell Signaling), insulin receptor β-subunit (1:1,000, 05-1104; Millipore), phospho-insulin receptor (Tyr1322) (1:200, 04-300; Millipore), IRS-2 (1:1,000, #4502; Cell Signaling), phospho-IRS-1/2 (Tyr612) (1:500, sc-17195; Santa Cruz Biotechnology), mature-form SREBP1 (1:1,000, NB100-60545; Novus Biologicals), carbohydrate responsive element–binding protein (ChREBP) (1:1,000, NB400-135, Novus Biologicals), phospho-FoxO1 (Ser256) (1:1,000, #9461; Cell Signaling), FoxO1 (1:1,000, #2880; Cell Signaling), and rictor (1:1,000, #2140; Cell Signaling).

Quantitative RT-PCR

Total RNA was isolated using RNeasy Mini Kit plus RNase-Free DNase treatment (QIAGEN). First-strand cDNA was generated using TaqMan Reverse Transcription Reagent. Quantitative PCR was carried out by using a StepOnePlus Real-Time PCR System (Applied Biosystems) with the Power SYBR Green PCR Master Mix (Applied Biosystems). Primer sequences are available upon request. Data were calibrated to endogenous control Actb or Hprt1, and the relative gene expression was quantified using the $2^{-\Delta\Delta CT}$ method (16).

Hepatocyte Isolation and Glucose Output Assay

Mouse hepatocytes were isolated from chow-fed wild-type mice 4 days after tail vein injection of Rec2-Ad36E4ORF1 (2×10^{10} vg/mouse) or AAV buffer as a control according to the published method with modifications (17). Briefly, mice were anesthetized and perfused at a rate of 3 mL/min by cannulation through the inferior vena cava with perfusion buffer (115 mmol/L NaCl, 5 mmol/L KCl, 25 mmol/L HEPES, 0.5 mmol/L EGTA, and 25 mmol/L D-glucose, pH 7.4) followed by Liver Digestion Medium (Thermo Fisher Scientific). The portal vein was cut to allow the flow of the solution through the liver. The perfusion temperature was kept at 37°C. The liver was dissected, and the capsule peeled off. Hepatocytes were dispersed by mechanical dissociation and filtered through a 100-μm strainer. The hepatocytes were rinsed twice in ice-cold DMEM supplemented with 10% FBS, penicillin/streptomycin, 10 nmol/L insulin, and 100 nmol/L dexamethasone; resuspended in the same culture medium; and then seeded in a collagen-coated six-well plate. The cell culture was continued for 24 h before starved overnight in serum-free DMEM without insulin and dexamethasone. The glucose output was measured in glucose- and phenol red–free DMEM supplemented with 20 mmol/L sodium lactate and 2 mmol/L sodium pyruvate. After a 5-h incubation, the supernatant medium was collected and briefly spun. The glucose concentration in the medium was determined by colorimetric glucose assay (Eton Bioscience, San Diego, CA). The glucose readout was normalized to the total protein content from each well cell lysate.

Oil Red O Staining

Lipids in liver were stained on frozen sections with an Oil Red O solution (Sigma).

Statistical Analysis

Data are expressed as mean ± SEM. We used JMP software to analyze the following: Student *t* test for comparison between two groups and one-way ANOVA for multiple group data followed by a post hoc test. Multivariate ANOVA was used to analyze quantitative RT-PCR data.

RESULTS

The Effects of Ad36E4ORF1 in Diabetes Model *db/db* Mice

In a pilot study, we administered rAAV-green fluorescent protein and rAAV-Ad36E4ORF1 to mice through a single tail vein injection (2×10^{10} vg/mouse) and sacrificed the animals 6 days postinjection. Intravenous delivery of AAV serotype Rec2 preferentially transduced liver. Green fluorescent protein fluorescence was observed in the liver (Supplementary Fig. 1*A*), and Ad36E4ORF1 expression was confirmed by Western blot (Supplementary Fig. 1*B*). No Ad36E4ORF1 was found in heart, kidney, or skeletal muscle or in white fat (Supplementary Fig. 1*B*).

To investigate the therapeutic potential of Ad36E4ORF1, we administered rAAV-Ad36E4ORF1 to the genetic model of diabetes and obesity *db/db* mice (2×10^{10} vg/mouse, single dose, tail vein injection). To study whether the effects were conserved among the E4ORF1 genes of other human adenoviruses, we generated an rAAV vector to express

Ad5E4ORF1 with the same expression cassette. dsYFP and AAV buffer were used as controls. No difference was observed between dsYFP and AAV buffer; therefore, the two groups were combined as a control group (data not shown). The mice treated with Ad5E4ORF1 showed decreased body weight by day 16 (Fig. 1*A*). Both Ad5E4ORF1- and Ad36E4ORF1-treated mice showed slight, but significant reduced food intake (Fig. 1*B*). Nonfasting blood glucose level was monitored periodically starting from day 6. Ad36E4ORF1-treated mice showed significantly reduced blood glucose levels by day 13, and the normalized blood glucose level was maintained throughout the rest of the experiment (Fig. 1*C*). In contrast, Ad5E4ORF1 treatment did not relieve hyperglycemia over the 4 weeks of the experiment (Fig. 1*C*). At 3 weeks post-AAV injection, a GTT was performed after an overnight fast. Ad36E4ORF1 treatment significantly reduced fasting blood glucose levels and robustly improved glycemic control (Fig. 1*D*). Most of the control- and Ad5E4ORF1-treated mice had blood glucose levels exceeding the glucose meter range and, therefore, were assigned 600 mg/dL at 30 min after glucose injection. Thus, the extent of reduced blood glucose level by Ad36E4ORF1 was underestimated at this time point. In addition, Ad36E4ORF1-treated mice showed reduced insulin levels at all time points during GTT (Fig. 1*E*). The amount of plasma insulin per unit glucose was significantly lower in the Ad36E4ORF1 group than in the control group at 30, 60, and 90 min of the GTT (Fig. 1*F*). Ad36E4ORF1 treatment did not change liver mass or fat mass (Fig. 1*G*). We repeated the experiment to measure the in vivo glucose uptake during a GTT by using glucose analog tracer 2-DG 8 weeks after rAAV injection. Ad36E4ORF1 treatment significantly increased liver glucose uptake but not skeletal muscle or fat uptake (Fig. 1*H*). We repeated the experiment once more to measure blood glucose level more accurately by using a glucose meter that reads up to 900 mg/dL. Hepatic expression of Ad36E4ORF1 robustly improved GTT (Supplementary Fig. 2*A*). An ITT was performed (Supplementary Fig. 2*B* and *C*). Ad36E4ORF1 treatment showed no effect on normalized blood glucose level during the ITT (Supplementary Fig. 2*C*), consistent with insulin-sparing action.

The serum levels of metabolites were measured at sacrifice 4 weeks after rAAV injection. The Ad36E4ORF1 group showed a significant reduction of glucose, insulin, and adiponectin, whereas a trend triglyceride reduction and cholesterol elevation in the circulation was found (Table 1). No changes were found in the serum levels of free fatty acids or leptin (Table 1). The liver function panel is shown in Supplementary Table 1. Among the liver metabolites measured, Ad36E4ORF1 treatment significantly increased acetyl-CoA level (Fig. 1*I*).

Ad36E4ORF1 Modulated Hepatic Gene Expression

We selected genes involved in glucose metabolism, lipid metabolism, and inflammation for the quantitative RT-PCR analysis of liver samples from control-, Ad5E4ORF1-, and Ad36E4ORF1-treated *db*/*db* mice (Fig. 2*A*). No changes of the expression of insulin receptor (Insr), GLUT2, or GLUT4 were observed (Fig. 2*A*). Ad36E4ORF1 selectively upregulated the expression of genes involved in glycolysis (Hk2 encoding hexokinase 2 and Pgam2 encoding phosphoglycerate mutase 2), whereas it did not change the expression of genes involved in gluconeogenesis (G6pc encoding glucose-6-phosphatase and Pck1 encoding PEPCK-1), glycogen synthesis (Gys encoding glycogen synthase 2), and pentose phosphate pathway (G6pdx encoding glucose-6-phosphate dehydrogenase X-linked, Pgd encoding phosphogluconate dehydrogenase, Rpe encoding ribulose-5-phosphate-3-epimerase). Pyruvate dehydrogenase kinase isoenzyme 4 (encoded by Pdk4) involved in the conversion of lactate to acetyl-CoA was upregulated by Ad5E4ORF1 but not Ad36E4ORF1 (Fig. 2*A*). Gck expression at the mRNA level was upregulated by Ad36E4ORF1 (Fig. 2*A*), and the protein level of this enzyme that is critically involved in controlling blood glucose levels was significantly increased more than twofold in Ad36E4ORF1-treated mice (Fig. 1*J*). Ad36E4ORF1 modulated a number of genes involved in lipogenesis and lipid oxidation (Fig. 2*A*). Two major transcription factors known to regulate de novo lipogenesis enzymes, SREBP1C (encoded by Srebf1c) and ChREBP (also known as MLXIPL), were measured (18,19). Ad36E4ORF1 significantly downregulated both the canonical ChREBP-α and the more potent isoform ChREBP-β (Fig. 2*A*). This downregulation of ChREBP was associated with downregulation of its lipogenic targets, including Acaca (encoding acetyl-CoA carboxylase α) and Gpd1 (encoding glycerol-3-phosphate dehydrogenase 1), which are required for triglyceride synthesis (20). In addition, Acox1 (encoding acyl-CoA oxidase 1), Cpt1a (encoding carnitine palmitoyltransferase 1A), and Ppara (encoding peroxisome proliferator–activated receptor α), genes involved in β-oxidation, were downregulated in Ad36E4ORF1-treated mice (Fig. 2*A*). Ad5E4ORF1 treatment showed significant downregulation of lipogenic transcription factors Chrebpa, Chrebpb, and Srebf1c, and lipogenic target Gpat (encoding glycerol-3-phosphate acyltransferase) (Fig. 2*A*). Both Ad5E4ORF1 and Ad36E4ORF1 were associated with induction of genes associated with inflammation, including Pai1 (encoding plasminogen activator inhibitor-1) and Ccl2 (encoding MCP-1) (Supplementary Fig. 4*A*). Hypothalamic expression of the genes involved in the regulation of energy balance was profiled by quantitative RT-PCR (Supplementary Fig. 3).

Ad36E4ORF1-Activated AKT Independent of Ras or Myc

In vitro data have shown that Ad36E4ORF1 upregulates Ras, leading to the activation of PI3K and AKT2 (6). We investigated the signaling pathways in the livers by Western blot. Ad36E4ORF1 transduction had no significant impact on insulin receptor, IRS-2, Ras, Myc, rictor, or phospho-FoxO1 (Fig. 3*A*). However, phospho-AKT at both Ser473 and Thr308 were significantly induced in Ad36E4ORF1-transduced liver (Fig. 3*A*).

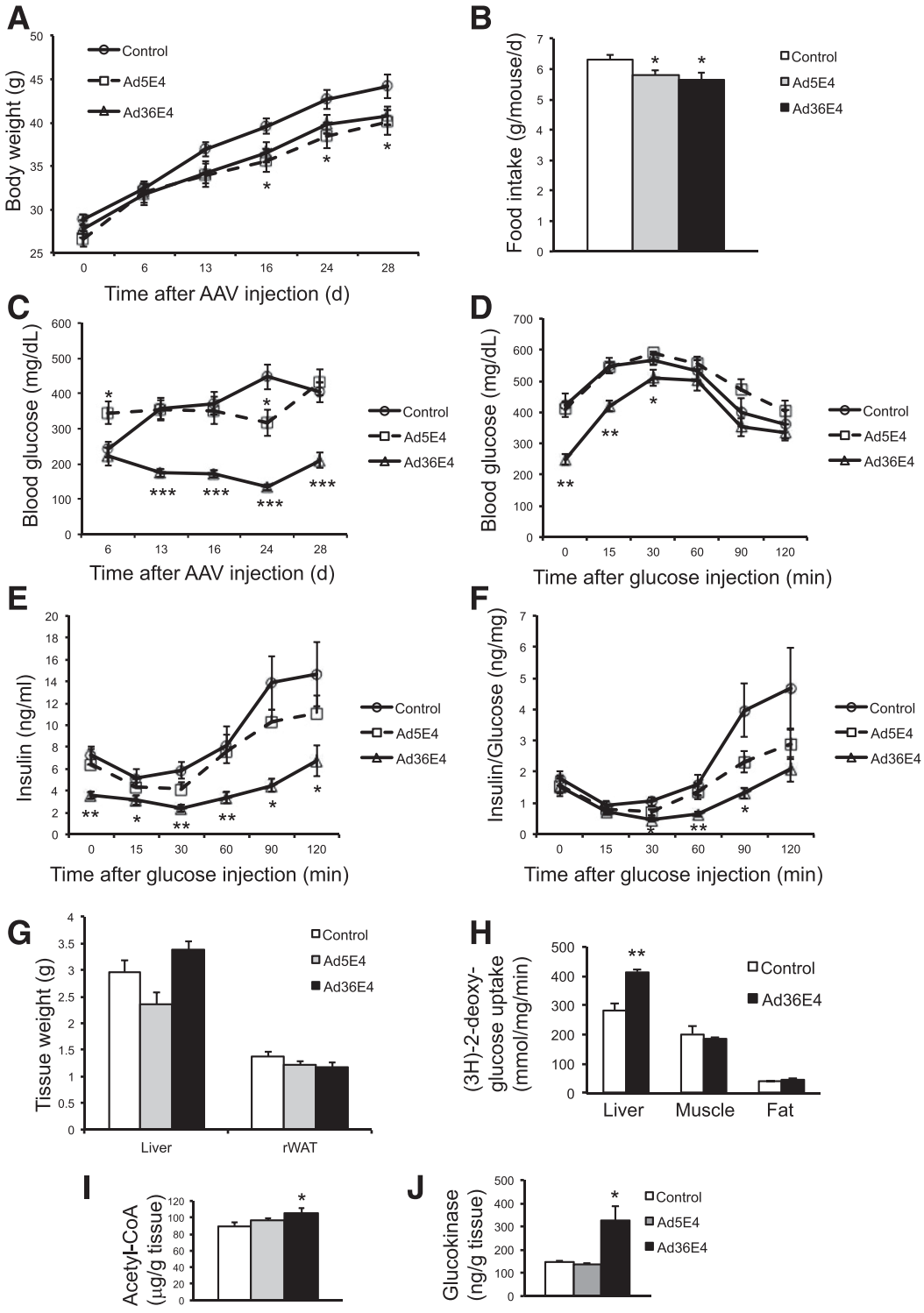

Figure 1—Ad36E4ORF1 alleviates hyperglycemia in *db/db* mice. *A*: Body weight of mice treated with rAAV-Ad36E4ORF1 (n = 8), rAAV-Ad5E4ORF1 (n = 8), or control (n = 8, combination of dsYFP and AAV buffer). *P < 0.05, Ad36E4ORF1 vs. control mice. *B*: Food intake. *C*: Nonfasting blood glucose levels. *D*: GTT after overnight fast. *E*: Serum insulin during GTT. *F*: Insulin/glucose ratio. *G*: Tissue weights. Data are mean ± SEM (n = 8/group). *H*: Glucose update assay in liver tissues from *db/db* mice 8 weeks after rAAV-Ad36E4ORF1 injection in a separate experiment (n = 4/group). *I*: Acetyl-CoA level in liver tissues (n = 8/group). *J*: GCK assay of liver (n = 4 control, n = 3 Ad5E4ORF1, and n = 4 Ad36E4ORF1). *P < 0.05; **P < 0.01; ***P < 0.001. rWAT, retroperitoneal white adipose tissue.

Table 1—Metabolic parameters in *db/db* mice and DIO mice

	db/db mice			DIO mice		
Parameter	Control	Ad5E4ORF1	Ad36E4ORF1	Control	Ad5E4ORF1	Ad36E4ORF1
Serum glucose (mg/dL)	470 ± 61.2	424 ± 51.6	292 ± 32.4*	225.9 ± 16.0	182.3 ± 11.3*	172.8 ± 14.8*
Serum insulin (ng/mL)	17.7 ± 4.2	5.0 ± 1.4*	5.5 ± 2.1*	1.73 ± 0.22	1.01 ± 0.28	0.37 ± 0.21***
Serum cholesterol (mg/dL)	80.5 ± 9.4	83.2 ± 8.4	106.4 ± 9.8	176.9 ± 18.3	139.6 ± 12.2	168.4 ± 15.5
Serum triglycerides (mg/dL)	159.1 ± 36.9	102.8 ± 9.4	79.0 ± 9.4	99.8 ± 9.4	92.7 ± 10.3	59.7 ± 7.3**
Serum NEFA (mEQ/L)	0.45 ± 0.05	0.44 ± 0.06	0.41 ± 0.03	0.36 ± 0.03	0.31 ± 0.04	0.30 ± 0.04
Serum leptin (ng/mL)	49.3 ± 4.3	43.8 ± 4.3	51.2 ± 5.6	20.0 ± 1.0	14.2 ± 1.4**	3.8 ± 1.0***
Serum adiponectin (μg/mL)	6.4 ± 0.6	5.4 ± 0.5	4.4 ± 0.4*	12.0 ± 0.6	10.4 ± 0.4	8.2 ± 0.6***
Liver cholesterol (mg/g)	10.3 ± 1.3	13.5 ± 1.1	13.3 ± 1.0	15.6 ± 3.0	14.8 ± 3.1	16.1 ± 2.4
Liver triglycerides (mg/g)	149.1 ± 9.4	173.4 ± 9.4	186.6 ± 9.4	113.9 ± 38.5	136.8 ± 39.3	262.5 ± 21.8**
Liver NEFA (mEQ/g)	0.24 ± 0.02	0.20 ± 0.01	0.21 ± 0.3	0.16 ± 0.01	0.16 ± 0.01	0.15 ± 0.01
Liver glycogen (mg/g)	7.49 ± 0.73	5.94 ± 0.15	6.20 ± 0.28	5.40 ± 0.38	4.54 ± 0.34	2.86 ± 0.10**

Data are mean ± SEM. $n = 8$ per group in *db/db* experiment. $n = 8$ control, 8 Ad5E4ORF1, and 9 Ad36E4ORF1 in DIO experiment. NEFA, nonesterified fatty acid. *$P < 0.05$, **$P < 0.01$, ***$P < 0.001$ vs. control.

The Effects of Ad36E4ORF1 in DIO Mice

We next investigated the effects of Ad36E4ORF1 in the DIO model that was insulin resistant but not hyperglycemic. The DIO mice were randomly assigned to receive rAAV-Ad36E4ORF1, Ad5E4ORF1, or dsYFP (2×10^{10} vg/mouse, single dose, tail vein injection). Ad36E4ORF1 treatment progressively decreased body weight by week 5 after rAAV injection (Fig. 4*A*), with no change in food intake (Fig. 4*B*). Nonfasting blood glucose level was monitored starting from 2 weeks after AAV injection. Ad36E4ORF1 treatment slightly, but significantly reduced blood glucose levels compared with control mice at some time points (Fig. 4*C*). A GTT was performed 3 weeks after AAV injection. Fasting blood glucose level in Ad36E4ORF1-treated mice was decreased compared with control mice. Furthermore, Ad36E4ORF1 mice displayed significantly improved glycemic control during GTT (Fig. 4*D*). Ad5E4ORF1-treated mice also showed improved GTT compared with control mice, although to a milder degree than Ad36E4ORF1. When the blood glucose changes were calibrated to baseline, only Ad36E4ORF1 mice showed significant differences (Fig. 4*E*). Mice were sacrificed 7 weeks after AAV injection. Ad36E4ORF1 mice showed increased liver weight but decreased adiposity (Fig. 4*F*).

Ad36E4ORF1 treatment resulted in a significant reduction of serum levels of glucose, insulin, leptin, adiponectin, and triglycerides (Table 1). However, triglyceride level in liver was significantly increased in Ad36E4ORF1-treated mice consistent with enlarged liver (Table 1). Liver glycogen level was reduced in Ad36E4ORF1 mice (Table 1). The expression of the same set of genes as the *db/db* mouse study was analyzed by quantitative RT-PCR (Fig. 2*B*). In the DIO model, Ad36E4ORF1 transduction led to upregulation of genes involved in glycolysis, including Hk2, Pgam2, and Pfkfb3 (encoding 6-phosphofructo-2-kinase/fructose-2,6-biphosphatase 3). Ad36E4ORF1 downregulated G6pc (Fig. 2*B*), which was not observed in *db/db* mice (Fig. 2*A*). The contribution of gluconeogenesis suppression to the improvement of glycemic control requires further investigation. In contrast to *db/db* mice, Ad36E4ORF1-treated DIO mice showed selective induction of lipogenic genes, including Scd2 (encoding stearoyl-CoA desaturase 2) and Gpd1 (Fig. 2*B*). Inflammation markers were induced in Ad36E4ORF1-transduced liver (Supplementary Fig. 4*B*). Similar to *db/db* mice, Ad36E4ORF1 transduction activated AKT signaling independent of insulin receptor or Ras (Fig. 3*B*).

Effects of Ad36E4ORF1 in Normal Wild-Type Mice

To further study the efficacy of Ad36E4ORF1 dose, we tested two doses in normal wild-type mice (2×10^9 and 2×10^{10} vg/mouse). Body weight was monitored daily and showed no changes (Fig. 5*A*). Nonfasting blood glucose level was monitored starting day 5 after AAV injection. Only high-dose (2×10^{10} vg/mouse) Ad36E4ORF1 mice showed a progressive decrease of blood glucose level (Fig. 5*B*). One week after rAAV injection, mice were sacrificed. Only the high-dose Ad36E4ORF1 mice showed a significant increase in liver mass (Fig. 5*C*). No change in the abdominal fat pad weight was observed (Fig. 5*C*). Dose-dependent Ad36E4ORF1 expression was confirmed by Western blot (Fig. 3*C*), and dose-dependent effects on serum metabolites were observed. High-dose Ad36E4ORF1 mice showed significantly decreased glucose but increased fatty acid and triglyceride levels among all groups (Table 2). Leptin level was not changed (Table 2), which is consistent with minimal transgene expression in the adipose tissue at the doses used (data not shown) and lack of impact on adipose tissue (Supplementary Fig. 5). We repeated the high-dose Ad36E4ORF1 experiment to isolate hepatocytes for the glucose output assay. Ad36E4ORF1 expression was confirmed by Western blot (data not shown). Ad36E4ORF1 expression did not change hepatocyte glucose output (Fig. 5*D*). Ad5E4ORF1 showed no changes in liver mass or serum metabolites (Fig. 5*C* and Table 2) even at a high dose,

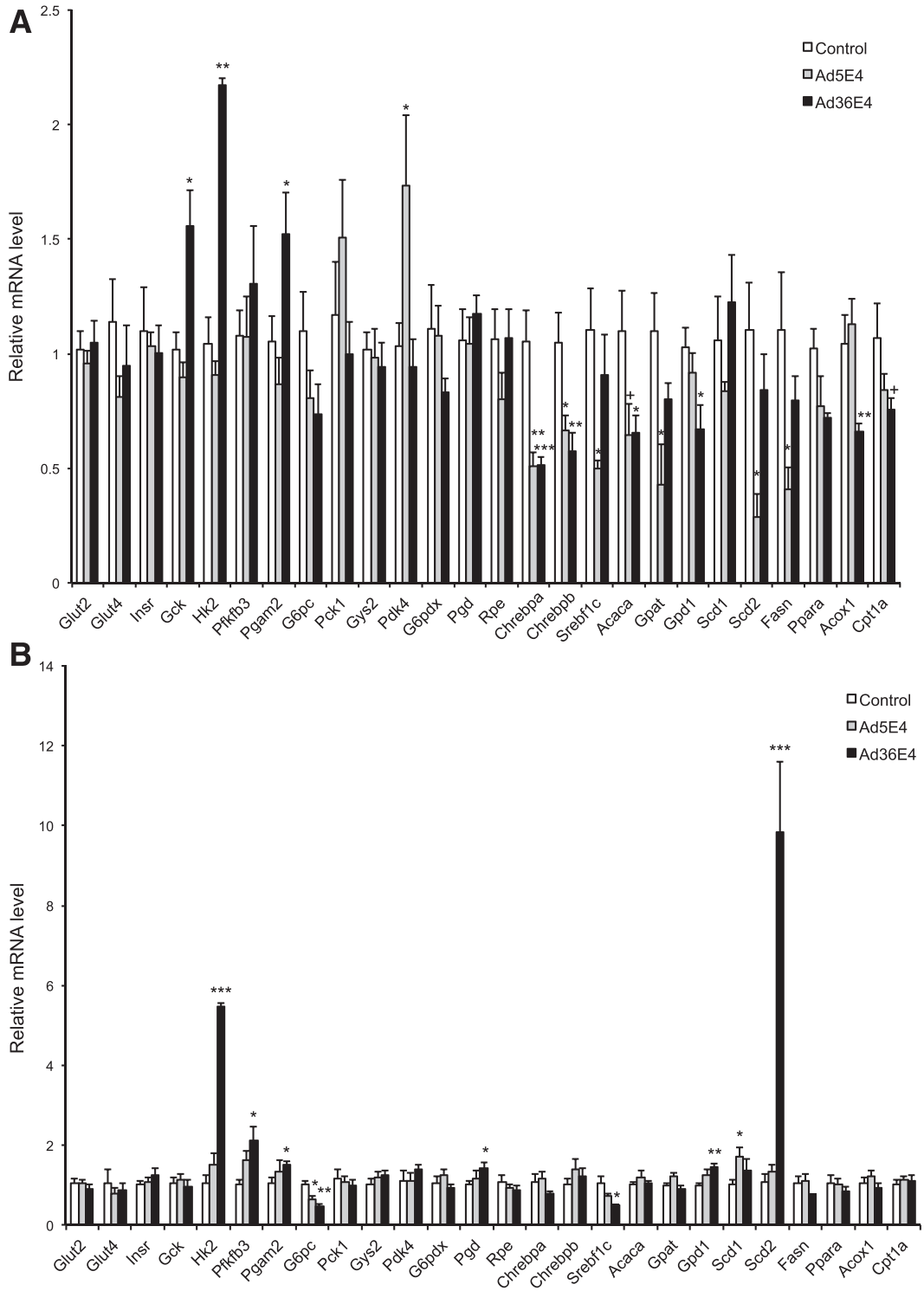

Figure 2—Ad36E4ORF1 modulates hepatic gene expression in *db/db* mice and DIO mice. *A*: *db/db* mice (n = 8 control, 5 Ad5E4ORF1, and 5 Ad36E4ORF1). *B*: DIO mice (n = 5/group). Data are mean ± SEM. *P < 0.05; **P < 0.01; ***P < 0.001; +P = 0.06.

although the transgene expression level was comparable to that of Ad36E4ORF1 at the same dose as measured by gene expression of woodchuck posttranscriptional regulatory element in all rAAV vectors (data not shown).

Liver cholesterol levels were not changed among all the groups (Table 2). The liver triglyceride level was increased in high-dose Ad36E4ORF1 mice by ~4.5-fold compared with dsYFP control, indicating that the lipid associated

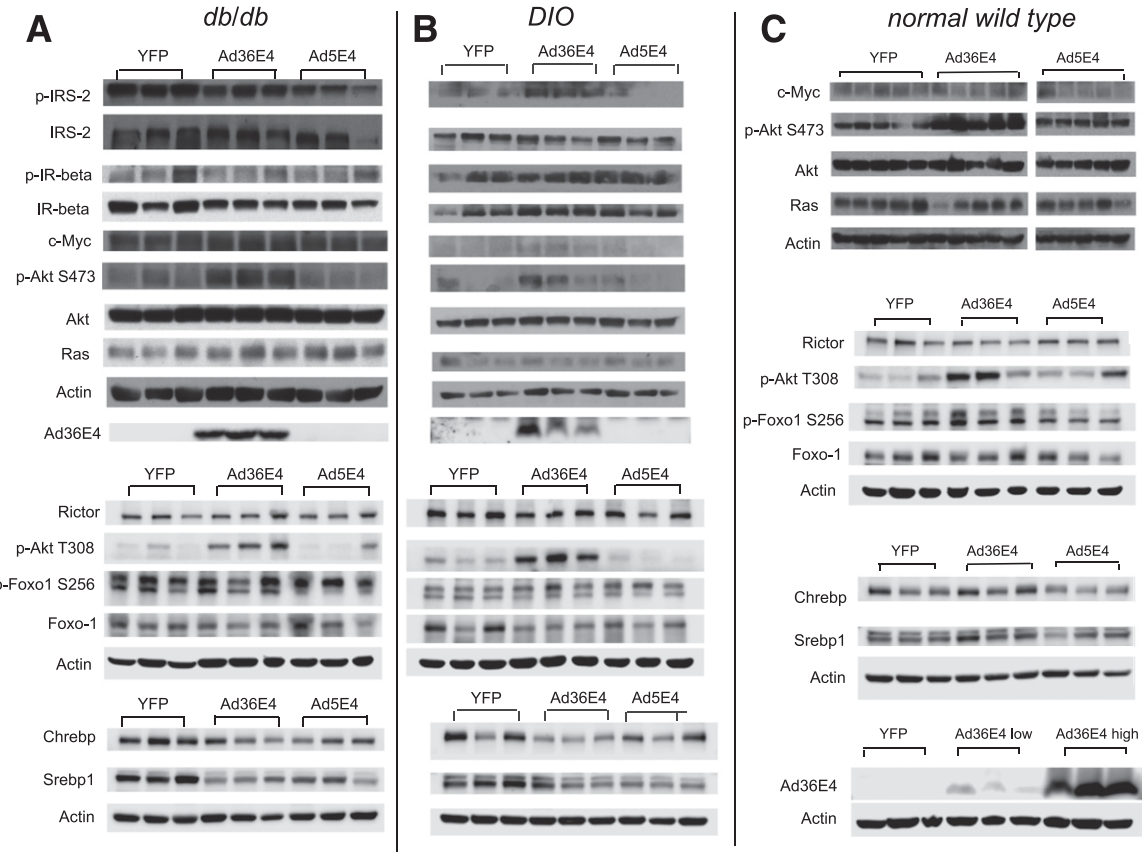

Figure 3—Signaling pathways and transcriptional factors in livers transduced by Ad36E4ORF1 in *db/db* (*A*), DIO (*B*), and normal wild-type (*C*) mice. Quantification of Western blots is provided in Supplementary Tables 2–4.

with fatty liver was primarily triglyceride (Table 2). High-dose Ad36E4ORF1 led to increased fatty acid while reducing glycogen levels in the liver (Table 2). Of note, Ad5E4ORF1 at a high dose elevated fatty acid levels in the liver (Table 2).

Gene expression profiling was performed on liver samples from dsYFP, high-dose Ad5E4ORF1, and both doses of Ad36E4ORF1 (Fig. 5*E*). High-dose Ad36E4ORF1 showed significant downregulation of Insr consistent with the suppression of proximal insulin signaling by Ad36 viral infection (21). High-dose Ad36E4ORF1 upregulated the expression of genes involved in glycolysis and downregulated genes involved in gluconeogenesis. Pdk4 involved in lactate conversion was upregulated by high-dose Ad36E4ORF1 (Fig. 5*E*). Moreover, Gys2 was downregulated consistent with the reduced level of glycogen in the livers transduced by high-dose Ad36E4ORF1 (Fig. 5*E* and Table 2). G6pdx involved in pentose phosphate pathway was downregulated (Fig. 5*E*). Among genes involved in lipid metabolism or associated with fatty liver, the effects of Ad36E4ORF1 were also dose dependent (Fig. 5*E*). Low-dose Ad36E4ORF1 significantly upregulated ChREBP-β (Fig. 5*E*). In the adipose tissue, the expression of the canonical ChREBP-α isoform is not regulated by glucose flux. However, glucose-induced ChREBP-α transcriptional activity increases ChREBP-β-expression, and ChREBP-β alone responds robustly to GLUT4-mediated changes in glucose flux (22). This upregulation of ChREBP-β by Ad36E4ORF1 was associated with a collective upregulation of its lipogenic targets, including Fasn (encoding fatty acid synthase), Acaca, Gpat, Gpd1, and Scd2 (Fig. 5*E*). Furthermore, Western blot confirmed the increase of ChREBP and the mature form of SREBP proteins (Fig. 3*C*). With the occurrence of hepatic steatosis in high-dose Ad36E4ORF1 mice, the expression of lipogenic transcription factors and fatty acid synthetic enzymes were downregulated, suggesting a negative feedback to the accumulation of triglycerides (Fig. 5*E*). In addition, Acox1, Cpt1a, and Ppara, genes involved in β-oxidation, were downregulated (Fig. 5*E*). The hepatic steatosis in high-dose Ad36E4ORF1 was associated with robust induction of inflammatory genes, including Pai1 and Ccl2 (Supplementary Fig. 4*C*). In contrast to Ad36E4ORF1, high-dose Ad5E4ORF1 led to no induction of glycolytic genes (Fig. 5*E*) and limited induction of lipogenic genes (Fig. 5*E*) and inflammatory genes (Supplementary Fig. 4*C*).

We investigated the signaling pathways in the livers of low-dose Ad36E4ORF1, Ad5E4ORF1, and dsYFP controls by Western blot (Fig. 3*C*). Phospho-AKT at Ser473 and Thr308 was significantly increased in Ad36E4ORF1 (Fig. 3*C*). Furthermore, MYC was not upregulated by Ad5E4ORF1, which was inconsistent with in vitro data (10). Ad5E4ORF1 also

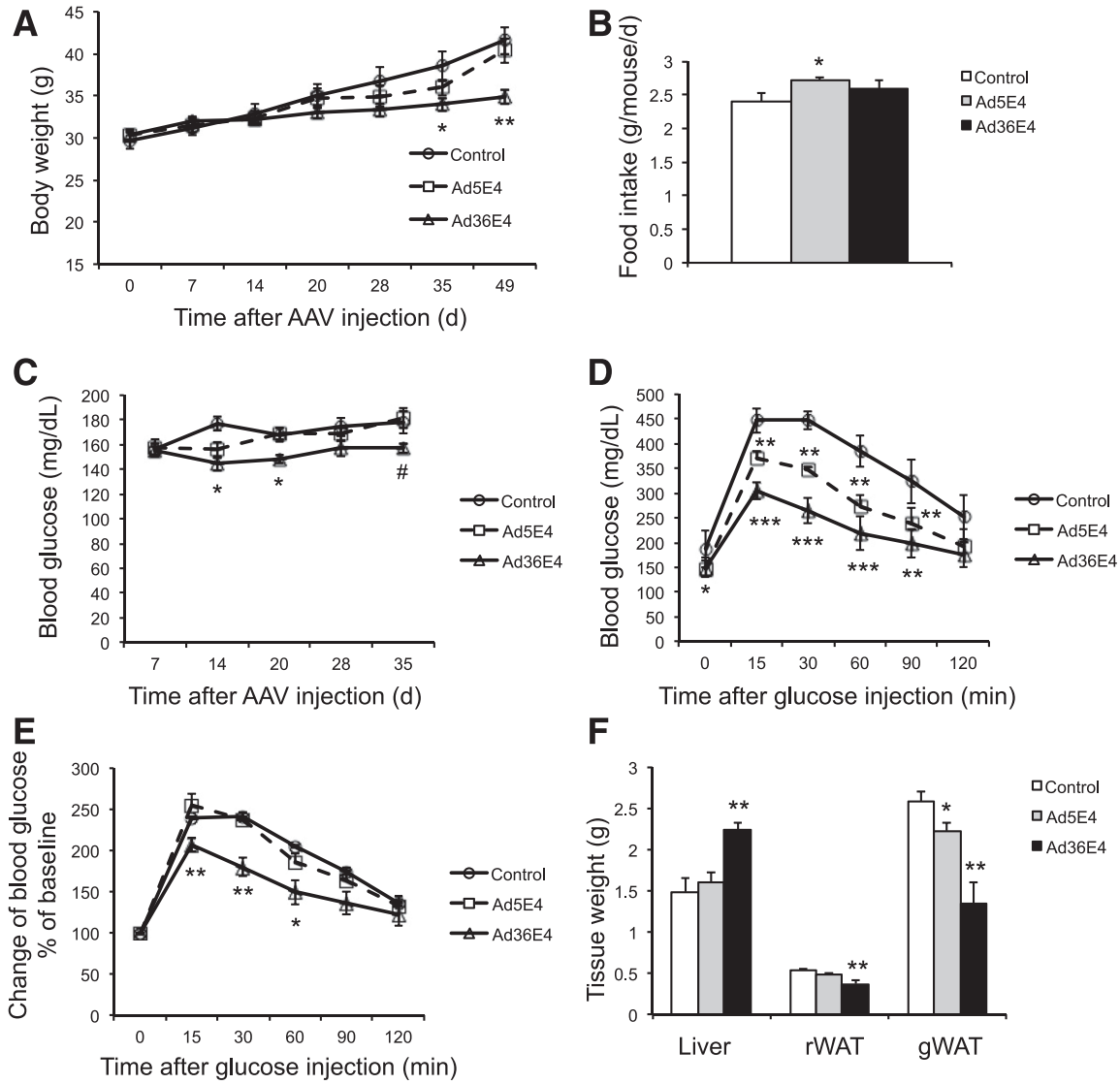

Figure 4—Ad36E4ORF1 improves glycemic control in DIO mice. *A*: Body weight. *B*: Food intake. *C*: Nonfasting blood glucose levels. *D*: GTT after overnight fast. *E*: Change in blood glucose calibrated to baseline during GTT. *F*: Tissue weight at sacrifice. Data are mean ± SEM (n = 8 control, n = 8 Ad5E4ORF1, and n = 9 Ad36E4ORF1). *P < 0.05, **P < 0.01, ***P < 0.001, #P = 0.07 vs. control. gWAT, gonadal white adipose tissue; rWAT, retroperitoneal white adipose tissue.

increased phospho-AKT, although the magnitude was less than Ad36E4ORF1 (Fig. 3*C*). Phospho-FoxO1 was increased in Ad36E4ORF1-transduced liver (Fig. 3*C*).

AKT Blockade Attenuates Ad36E4ORF1 Effects

To investigate the role of AKT activation in mediating Ad36E4ORF1 effects, perifosine, an oral bioactive alkylphospholipid, was used to inhibit AKT activation (23). Wild-type mice of normal weight were randomly assigned to receive rAAV-Ad36E4ORF1 (high dose of 2×10^{10} vg/mouse) or AAV buffer. Perifosine was given orally on days 4 and 5 to one-half of the Ad36E4ORF1 mice or control mice. Nonfasting blood glucose levels were monitored daily starting before the first dose of perifosine on day 4. Ad36E4ORF1-treated mice receiving oral PBS showed significantly decreased blood glucose levels on days 5 and 6. Perifosine prevented the lowering of glucose in Ad36E4ORF1-treated mice on day 5 and substantially attenuated the drop of blood glucose level on day 6 (Fig. 6*A*). Mice were sacrificed on day 6 after AAV injection. Hematoxylin-eosin and trichrome staining showed no hepatic toxicity associated with perifosine treatment (Fig. 6*D*). Perifosine significantly blocked the hepatomegaly induced by high-dose Ad36E4ORF1 (Fig. 6*B*) and substantially attenuated liver steatosis revealed by Oil Red O staining (Fig. 6*C* and *D*). Western blot confirmed the inhibition of AKT activation by perifosine (Fig. 6*E*).

DISCUSSION

Ad36 is one of the 56 serotypes in seven subgroups of human adenoviruses. Ad36 was the first human adipogenic

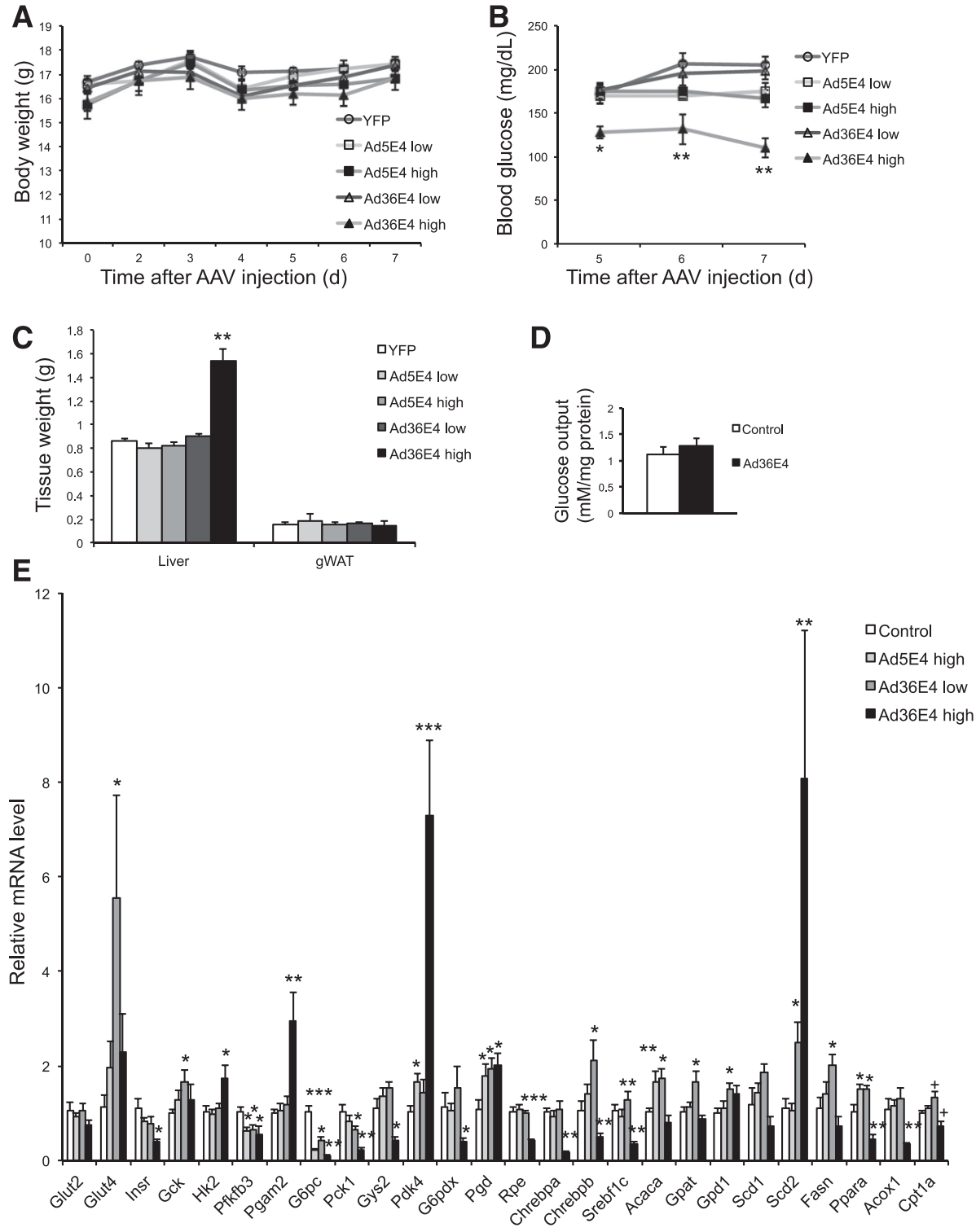

Figure 5— Dose-dependent effects of Ad36E4ORF1 in normal wild-type mice. *A*: Body weight. *B*: Nonfasting blood glucose level. *C*: Tissue weights at sacrifice. *D*: Hepatocyte glucose output assay. *E*: Hepatic gene expression (n = 5/group). Data are mean ± SEM. Low dose: 2×10^9 vg/mouse; high dose: 2×10^{10} vg/mouse. *$P < 0.05$, **$P < 0.01$, ***$P < 0.001$ vs. YFP; +$P = 0.06$. gWAT, gonadal white adipose tissue.

virus reported and the most investigated up to date. In various animal models, experimental infection of Ad36 increases obesity but improves glycemic control (24). Studies from many countries show that prior Ad36 exposure in humans, as determined by the presence of neutralizing antibodies to Ad36, is associated with an increased risk for obesity (25–32), better glycemic control (21,33), and lower hepatic lipid levels (26,27,34). Subsequent

Table 2—Metabolic parameters in normal wild-type mice

Parameter	YFP	Ad5E4ORF1 low	Ad5E4ORF1 high	Ad36E4ORF1 low	Ad36E4ORF1 high
Serum glucose (mg/dL)	226.5 ± 18.8	193.1 ± 12.3	210.1 ± 8.3	201.4 ± 8.6	146.6 ± 20.5**
Serum insulin (ng/mL)	0.71 ± 0.35	0.61 ± 0.15	0.53 ± 0.14	0.65 ± 0.17	0.29 ± 0.08
Serum cholesterol (mg/dL)	76.3 ± 6.7	90.5 ± 11.0	80.3 ± 7.8	98.6 ± 9.6	73.7 ± 11.0
Serum triglycerides (mg/dL)	75.6 ± 11.6	54.6 ± 5.6	74.6 ± 8.9	61.0 ± 4.2	137.9 ± 14.7**
Serum NEFA (mEQ/L)	0.41 ± 0.04	0.50 ± 0.04	0.48 ± 0.05	0.54 ± 0.12	0.80 ± 0.08
Serum leptin (ng/mL)	1.20 ± 0.29	1.73 ± 0.25	1.39 ± 0.35	1.95 ± 0.34	1.22 ± 0.38
Liver cholesterol (mg/g)	0.91 ± 0.07	0.96 ± 0.10	1.04 ± 0.15	0.74 ± 0.07	1.16 ± 0.25
Liver triglyceride (mg/g)	1.01 ± 0.11	1.30 ± 0.24	1.51 ± 0.21	1.74 ± 0.26	4.68 ± 0.82**
Liver NEFA (mEQ/g)	0.017 ± 0.002	0.014 ± 0.001	0.035 ± 0.002*	0.012 ± 0.001	0.041 ± 0.003**
Liver glycogen (mg/g)	83.8 ± 3.2	70.4 ± 5.4	75.7 ± 5.1	74.5 ± 3.1	51.1 ± 3.6**

Data are mean ± SEM. Low, 2×10^9 vg/mouse; high, 2×10^{10} vg/mouse. n = 5/group. NEFA, nonesterified fatty acid. *$P < 0.05$, **$P < 0.01$ vs. YFP.

in vitro studies attribute these effects of Ad36 to its E4ORF1 gene (6,7). These studies suggest the potential of E4ORF1 as a template for developing antidiabetic therapies (5,6,8,21).

Improvement in Glycemic Control

We tested the effect of hepatic expression of Ad36E4ORF1 in a genetic model of diabetes (*db/db* mice), dietary model of insulin resistance (DIO mice), and normoglycemia

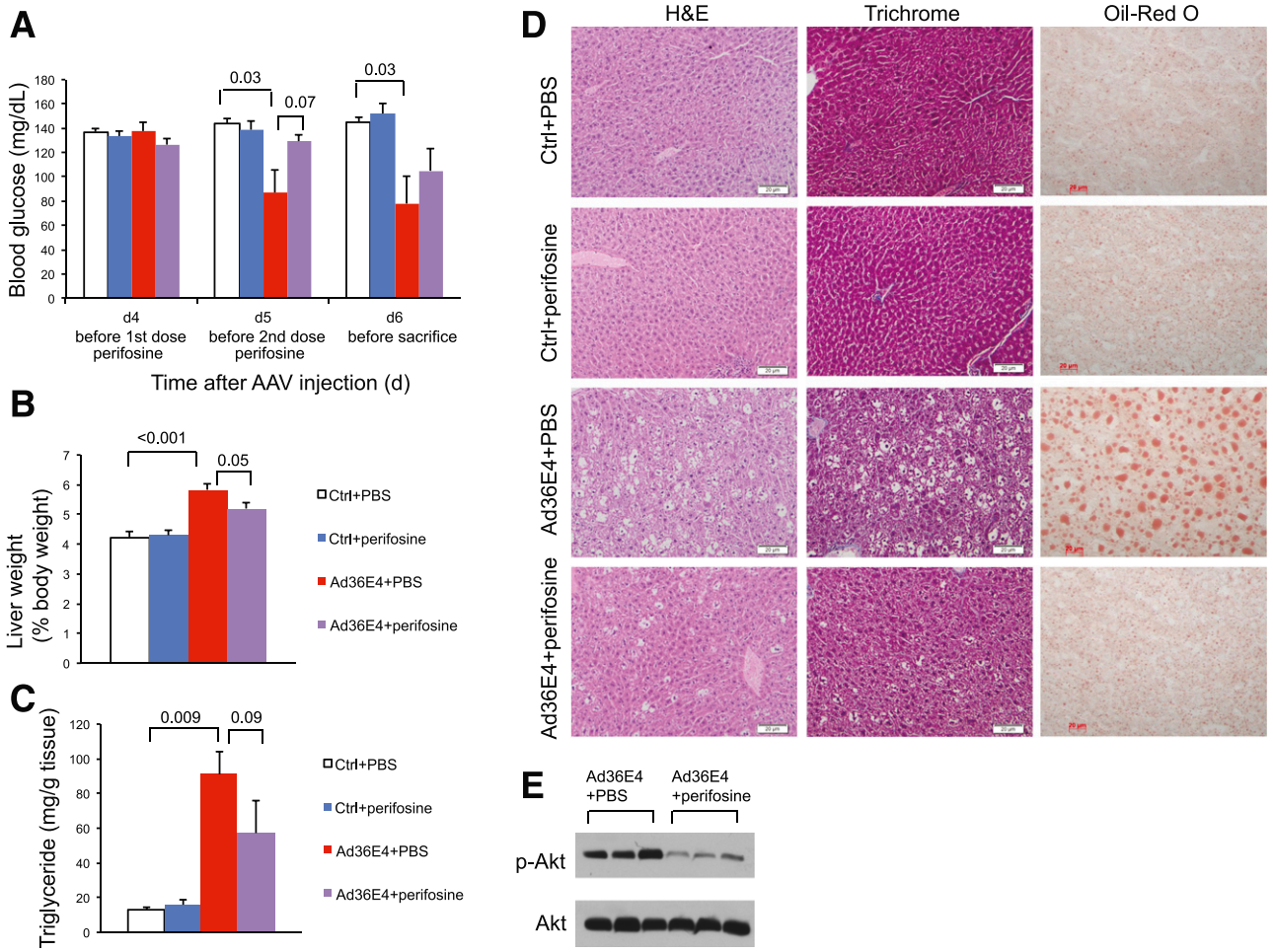

Figure 6—Perifosine attenuates the effects of Ad36E4ORF1 in normal wild-type mice. *A*: Nonfasting blood glucose levels. *B*: Liver weight calibrated to body weight at sacrifice. *C*: Liver triglyceride concentration. *D*: Hematoxylin-eosin (H&E), trichrome, and Oil Red O staining of livers. *E*: Western blots of livers. Data are mean ± SEM (n = 4–6/group). *P* values of significance or trend of significance are listed above the bars. Ctrl, control. Scale bars, 20 μm.

(wild-type mice). In the diabetes model, rAAV-Ad36E4ORF1 treatment completely alleviated hyperglycemia (>70%) (Fig. 1*C*) and robustly improved glycemic control during GTT without significantly increasing hepatic steatosis. In the DIO model, Ad36E4ORF1 reduced blood glucose levels but did not cause hypoglycemia and significantly improved GTT. Finally, in normoglycemic mice, hepatic expression of Ad36E4ORF1 at a higher level lowered nonfasting blood glucose. Of note, Ad36E4ORF1 significantly reduced insulin levels in *db/db* and DIO mice and showed a trend toward reduction in wild-type mice. The improvement in glycemic control was observed without stimulation of the proximal insulin signaling (insulin receptor, IRS-2). Collectively, these data indicate that Ad36E4ORF1 is not a typical sensitizer, mimetic, or secretagogue of insulin. Instead, it appears to have an insulin-sparing action (9), which reduces the need for insulin and, hence, reduces insulin levels.

Although Ad36E4ORF1 does not induce proximal insulin signaling, it activates the distal insulin signaling involving AKT through the activation of Ras in vitro (6). However, Ad36E4ORF1 expression in the livers of all mouse models did not upregulate Ras. Yet, in agreement with in vitro data, among all the models tested, Ad36E4ORF1 activated AKT independently of proximal insulin receptor signaling. The requirement of AKT for Ad36E4ORF1-induced modulation of glucose levels was demonstrated by inhibiting AKT activation with perifosine, which attenuated the lowering of glucose. The mechanisms of Ad36E4ORF1 induction of phospho-AKT independent of Ras remain to be elucidated. Complete activation of AKT is achieved by phosphorylation of both Thr308 and Ser473. Although Thre308 andSer473 are catalyzed by separate kinases and occur independently of each other, both phosphorylation events require binding of AKT to PIP3 in response to PI3K signaling. Phosphorylation of both sites is required for catalytically active AKT to properly dissociate from the membrane and phosphorylate downstream targets. AKT enters a catalytically active state when Thr308 is phosphorylated by PDK1 (35). AKT catalytic activity and substrate specificity are further enhanced when mTOR complex 2 (mTORC2) phosphorylates AKT at Ser473, an event that also requires association of AKT with PIP3 (36). Rictor is a core component of mTORC2 and is required for Ser473 phosphorylation (37). Two core proteins of mTORC2, rictor and SIN, not only are required for mTORC2 assembly but also prevent degradation of each other (38). Therefore, measurement of either provides a valid assessment of mTORC2 abundance. The current data show that rictor levels were unchanged in response to hepatic expression of Ad36E4ORF1 (Fig. 3). Moreover, liver-specific rictor knockout mice display dramatically reduced AKT phosphorylation at Ser473 but not at Thr308, indicating that only Ser473 is a target of mTORC2 (39). The current data show that hepatic Ad36E4ORF1 expression increases phosphorylation of AKT at Thr308 and Ser473, suggesting that mTORC2 function unlikely is increased to mediate Ad36E4ORF1-induced AKT activation. Taken together, phosphorylation of AKT likely is due to elevated PIP3 levels in response to E4ORF1-mediated PI3K activation similar to in vitro findings of highly homologous E4ORF1 protein from Ad9 (40,41).

Hepatic Steatosis

Ad36E4ORF1 increased liver weight and triglycerides in DIO and wild-type mice but not in *db/db* mice. On the basis of the data from gene expression profiling and liver metabolites, we propose that Ad36E4ORF1 acts on the cellular metabolism observed in the transduced liver of normoglycemic mice. Ad36E4ORF1 elevates glycolysis. The glycolytic intermediates are shunted mainly to triacylglycerol synthesis, whereas glycogen, lactate, ATP production, and nucleotide synthesis remain either slightly reduced or unchanged. Ad36E4ORF1 induces the expression of ChREBP-β, which is highly responsive to glucose influx and subsequently induces the lipogenic and glycolytic genes. The accumulation of triacylglycerol leads to steatosis.

Whether the effects on glycemic control and liver de novo lipogenesis can be dissociated could possibly depend on the basal AKT activation status in the liver as well as on the presence and severity of insulin resistance. For example, in *db/db* mice, AKT activity was decreased compared with wild-type mice (42). Therefore, Ad36E4ORF1 treatment could normalize the abnormally low AKT activity and subsequently improve glycemic control. However, in normal animals, overshooting AKT activation by Ad36E4ORF1 could lead to hepatic steatosis and hypoglycemia, a phenomenon similar to the PTEN mutants (43). Ad36E4ORF1 activated AKT, leading to an increase in hepatic glycolysis, yet glucose output and FOXO1 and its target gene PCK1 were unchanged. One would anticipate that activation of AKT would phosphorylate its target protein FOXO1 and therefore decrease FOXO1 activity and reduce gluconeogenesis. However, Ad36E4ORF1 upregulated inflammatory cytokines (Supplementary Fig. 4) in addition to steatosis. It has been shown that the expression and activity of FOXO1 are increased in nonalcoholic steatohepatitis (44). Therefore, the steatosis and increase of inflammatory cytokines are possibly associated with hepatic Ad36E4ORF1 expression, offsetting the effect of AKT activation on FOXO1.

Ad36 and E4ORF1

All serotypes of adenovirus have the E4ORF1 gene that shares the conserved amino acid domain with dUTPase but has distinct functionality (45). Ad5E4ORF1 is well characterized and mediates the reprogramming of cellular metabolism that mirrors the Warburg effect in cancer by enhancing MYC transcriptional activation of glycolytic genes and promoting glycolysis, resulting in increased nucleotide biosynthesis (10). The in vitro findings have yet to be confirmed in vivo. The amino acid homology between Ad5E4ORF1 and Ad36E4ORF1 is ~45%. The current data demonstrate that the effects of Ad36E4ORF1 are different from those of Ad5E4ORF1. In contrast to Ad36E4ORF1, Ad5E4ORF1 did not decrease blood glucose levels in normal animals or in *db/db* mice. Hepatic expression of Ad5E4ORF1 did not replicate

the increase of MYC observed in cell culture (10). The discrepancy could be due to the difference of transduced tissue and cell types. Of note, both Ad36E4ORF1 and Ad5E4ORF1 significantly activated AKT and promoted hepatic glycolysis in normal animals. Activation of the PI3K/AKT pathway is a well-documented function of E4ORF1 shared by several human adenoviruses and may contribute to tumorigenic property, promotion of survival, viral replication, or reprogramming of host cell metabolism, depending on adenovirus types and infected cells and tissues (6,10,46,47). E4ORF1 from Ad9 and Ad5 interacts with a select group of PDZ domain–containing cellular products (41,48,49). The extreme carboxy-terminal of E4ORF1 contains the crucial PDZ domain–binding motif essential for activation of PI3K/AKT signaling (10,40,50,51). Because the consensus X-S/T-X-(VLI) is conserved in Ad5-, Ad9-, and Ad36E4ORF1 (40), it is possible that the same motif in Ad36 participates in PI3K/AKT signaling. The Ad36 infection has not been linked to an increased risk of tumor formation in humans or animals. In addition, expression of Ad36E4ORF1 in the adipose tissue is not tumorigenic (9). However, given the potential tumorigenic effect of Ad9E4ORF1, investigating whether Ad36E4ORF1 and Ad9E4ORF1, which share a 92% amino acid homology, also share similar effects on cellular metabolism as well as oncogenesis is important. Our rAAV vector provides a powerful tool to study the short- and long-term effects of adenoviral genes in various tissues in vivo.

This proof-of-concept study shows that predominant hepatic expression of Ad36E4ORF1 alleviates hyperglycemia in genetic models of diabetes and diet-induced insulin resistance, and this property may not be shared by the E4ORF1 genes of all human adenoviruses. The insulin-sparing action of Ad36E4ORF1 is particularly attractive. How the hepatic response would be modulated is unknown due to secondary input from other tissues if they were to also express E4ORF1. Nonetheless, the amount of E4ORF1 expression in liver appears to have a threshold that should not be exceeded. Future studies with detailed analyses on glycemic control in animal models of hyperglycemia should further characterize the phenomenon.

Funding. The study was supported in part by National Cancer Institute grants CA-166590, CA-178227, and CA-163640 to L.C.

Duality of Interest. N.V.D. has been granted or has applied for the following patents: 6,127,113; 6,664,050; and 8,008,436B2. The provisional patent Adenovirus Ad36 E4orf1 Protein for Prevention and Treatment of Non-alcoholic Fatty Liver Disease was filed July 2010, and the provisional patent Enhanced Glycemic Control Using Ad36E4orf1 and AKT1 Inhibitor was filed January 2012. N.V.D. has ongoing grant support from Vital Health Interventions for determining antidiabetic properties of the E4ORF1 protein. No other potential conflicts of interest relevant to this article were reported.

Author Contributions. T.B.M. and W.H. conducted experiments, analyzed data, and revised the manuscript. R.X. and X.L. conducted experiments and analyzed data. N.V.D. provided materials, advised experiments, and contributed to the writing and revision of the manuscript. L.C. conceived of the study design, conducted experiments, analyzed data, and wrote and revised the manuscript. L.C. is the guarantor of this work and, as such, had full access to all the data in the study and takes responsibility for the integrity of the data and the accuracy of the data analysis.

References

1. Draznin B. Molecular mechanisms of insulin resistance: serine phosphorylation of insulin receptor substrate-1 and increased expression of p85alpha: the two sides of a coin. Diabetes 2006;55:2392–2397
2. Kovacs P, Hanson RL, Lee YH, et al. The role of insulin receptor substrate-1 gene (IRS1) in type 2 diabetes in Pima Indians. Diabetes 2003;52:3005–3009
3. Rung J, Cauchi S, Albrechtsen A, et al. Genetic variant near IRS1 is associated with type 2 diabetes, insulin resistance and hyperinsulinemia. Nat Genet 2009;41:1110–1115
4. Danielsson A, Ost A, Lystedt E, et al. Insulin resistance in human adipocytes occurs downstream of IRS1 after surgical cell isolation but at the level of phosphorylation of IRS1 in type 2 diabetes. FEBS J 2005;272:141–151
5. Dhurandhar EJ, Dubuisson O, Mashtalir N, Krishnapuram R, Hegde V, Dhurandhar NV. E4orf1: a novel ligand that improves glucose disposal in cell culture. PLoS One 2011;6:e23394
6. Dhurandhar EJ, Krishnapuram R, Hegde V, et al. E4orf1 improves lipid and glucose metabolism in hepatocytes: a template to improve steatosis & hyperglycemia. PLoS One 2012;7:e47813
7. Krishnapuram R, Dhurandhar EJ, Dubuisson O, Hegde V, Dhurandhar NV. Doxycycline-regulated 3T3-L1 preadipocyte cell line with inducible, stable expression of adenoviral E4orf1 gene: a cell model to study insulin-independent glucose disposal. PLoS One 2013;8:e60651
8. Dhurandhar NV. Insulin sparing action of adenovirus 36 and its E4orf1 protein. J Diabetes Complications 2013;27:191–199
9. Kusminski CM, Gallardo-Montejano VI, Wang ZV, et al. E4orf1 induction in adipose tissue promotes insulin-independent signaling in the adipocyte. Mol Metab 2015;4:653–664
10. Thai M, Graham NA, Braas D, et al. Adenovirus E4ORF1-induced MYC activation promotes host cell anabolic glucose metabolism and virus replication. Cell Metab 2014;19:694–701
11. Liu X, Magee D, Wang C, et al. Adipose tissue insulin receptor knockdown via a new primate-derived hybrid recombinant AAV serotype. Mol Ther Methods Clin Dev 2014;1:1
12. Mauvais-Jarvis F, Virkamaki A, Michael MD, et al. A model to explore the interaction between muscle insulin resistance and beta-cell dysfunction in the development of type 2 diabetes. Diabetes 2000;49:2126–2134
13. Boini KM, Graf D, Hennige AM, et al. Enhanced insulin sensitivity of gene-targeted mice lacking functional KCNQ1. Am J Physiol Regul Integr Comp Physiol 2009;296:R1695–R1701
14. Folch J, Lees M, Sloane Stanley GH. A simple method for the isolation and purification of total lipides from animal tissues. J Biol Chem 1957;226:497–509
15. Passonneau JV, Lauderdale VR. A comparison of three methods of glycogen measurement in tissues. Anal Biochem 1974;60:405–412
16. Livak KJ, Schmittgen TD. Analysis of relative gene expression data using real-time quantitative PCR and the 2(-delta delta C(T)) method. Methods 2001;25:402–408
17. Bocharov AV, Huang W, Vishniakova TG, et al. Glucocorticoids upregulate high-affinity, high-density lipoprotein binding sites in rat hepatocytes. Metabolism 1995;44:730–738
18. Horton JD, Goldstein JL, Brown MS. SREBPs: activators of the complete program of cholesterol and fatty acid synthesis in the liver. J Clin Invest 2002;109:1125–1131
19. Iizuka K, Bruick RK, Liang G, Horton JD, Uyeda K. Deficiency of carbohydrate response element-binding protein (ChREBP) reduces lipogenesis as well as glycolysis. Proc Natl Acad Sci U S A 2004;101:7281–7286
20. Sato T, Morita A, Mori N, Miura S. The role of glycerol-3-phosphate dehydrogenase 1 in the progression of fatty liver after acute ethanol administration in mice. Biochem Biophys Res Commun 2014;444:525–530
21. Krishnapuram R, Dhurandhar EJ, Dubuisson O, et al. Template to improve glycemic control without reducing adiposity or dietary fat. Am J Physiol Endocrinol Metab 2011;300:E779–E789
22. Herman MA, Peroni OD, Villoria J, et al. A novel ChREBP isoform in adipose tissue regulates systemic glucose metabolism. Nature 2012;484:333–338

23. Hideshima T, Catley L, Yasui H, et al. Perifosine, an oral bioactive novel alkylphospholipid, inhibits Akt and induces in vitro and in vivo cytotoxicity in human multiple myeloma cells. Blood 2006;107:4053–4062
24. Dhurandhar NV. A framework for identification of infections that contribute to human obesity. Lancet Infect Dis 2011;11:963–969
25. Atkinson RL, Dhurandhar NV, Allison DB, et al. Human adenovirus-36 is associated with increased body weight and paradoxical reduction of serum lipids. Int J Obes 2005;29:281–286
26. Trovato GM, Martines GF, Garozzo A, et al. Ad36 adipogenic adenovirus in human non-alcoholic fatty liver disease. Liver Int 2010;30:184–190
27. Trovato GM, Castro A, Tonzuso A, et al. Human obesity relationship with Ad36 adenovirus and insulin resistance. Int J Obes 2009;33:1402–1409
28. Almgren M, Atkinson R, He J, et al. Adenovirus-36 is associated with obesity in children and adults in Sweden as determined by rapid ELISA. PLoS One 2012;7:e41652
29. Na HN, Hong YM, Kim J, Kim HK, Jo I, Nam JH. Association between human adenovirus-36 and lipid disorders in Korean schoolchildren. Int J Obes 2010;34: 89–93
30. Gabbert C, Donohue M, Arnold J, Schwimmer JB. Adenovirus 36 and obesity in children and adolescents. Pediatrics 2010;126:721–726
31. Atkinson RL, Lee I, Shin HJ, He J. Human adenovirus-36 antibody status is associated with obesity in children. Int J Pediatr Obes 2010;5:157–160
32. Aldhoon-Hainerová I, Zamrazilová H, Atkinson RL, et al. Clinical and laboratory characteristics of 1179 Czech adolescents evaluated for antibodies to human adenovirus 36. Int J Obes 2014;38:285–291
33. Lin WY, Dubuisson O, Rubicz R, et al. Long-term changes in adiposity and glycemic control are associated with past adenovirus infection. Diabetes Care 2013;36:701–707
34. Trovato GM, Martines GF, Pirri C, et al. Obesity-independent association of human adenovirus Ad37 seropositivity with nonalcoholic fatty liver disease. J Clin Gastroenterol 2012;46:e46–e54
35. Chan TO, Rittenhouse SE, Tsichlis PN. AKT/PKB and other D3 phosphoinositide-regulated kinases: kinase activation by phosphoinositide-dependent phosphorylation. Annu Rev Biochem 1999;68;965–1014
36. Scheid MP, Marignani PA, Woodgett JR. Multiple phosphoinositide 3-kinase-dependent steps in activation of protein kinase B. Mol Cell Biol 2002; 22:6247–6260
37. Sarbassov DD, Guertin DA, Ali SM, Sabatini DM. Phosphorylation and regulation of Akt/PKB by the rictor-mTOR complex. Science 2005;307:1098–1101
38. Oh WJ, Jacinto E. mTOR complex 2 signaling and functions. Cell Cycle 2011;10:2305–2316
39. Hagiwara A, Cornu M, Cybulski N, et al. Hepatic mTORC2 activates glycolysis and lipogenesis through Akt, glucokinase, and SREBP1c. Cell Metab 2012;15:725–738
40. Frese KK, Lee SS, Thomas DL, et al. Selective PDZ protein-dependent stimulation of phosphatidylinositol 3-kinase by the adenovirus E4-ORF1 oncoprotein. Oncogene 2003;22:710–721
41. Kong K, Kumar M, Taruishi M, Javier RT. The human adenovirus E4-ORF1 protein subverts discs large 1 to mediate membrane recruitment and dysregulation of phosphatidylinositol 3-kinase. PLoS Pathog 2014;10:e1004102
42. Shao J, Yamashita H, Qiao L, Friedman JE. Decreased Akt kinase activity and insulin resistance in C57BL/KsJ-Leprdb/db mice. J Endocrinol 2000;167: 107–115
43. He L, Hou X, Kanel G, et al. The critical role of AKT2 in hepatic steatosis induced by PTEN loss. Am J Pathol 2010;176:2302–2308
44. Valenti L, Rametta R, Dongiovanni P, et al. Increased expression and activity of the transcription factor FOXO1 in nonalcoholic steatohepatitis. Diabetes 2008; 57:1355–1362
45. Weiss RS, Lee SS, Prasad BV, Javier RT. Human adenovirus early region 4 open reading frame 1 genes encode growth-transforming proteins that may be distantly related to dUTP pyrophosphatase enzymes. J Virol 1997;71:1857–1870
46. Seandel M, Butler JM, Kobayashi H, et al. Generation of a functional and durable vascular niche by the adenoviral E4ORF1 gene. Proc Natl Acad Sci U S A 2008;105:19288–19293
47. O'Shea C, Klupsch K, Choi S, et al. Adenoviral proteins mimic nutrient/growth signals to activate the mTOR pathway for viral replication. EMBO J 2005; 24:1211–1221
48. Chung SH, Frese KK, Weiss RS, Prasad BV, Javier RT. A new crucial protein interaction element that targets the adenovirus E4-ORF1 oncoprotein to membrane vesicles. J Virol 2007;81:4787–4797
49. Weiss RS, Javier RT. A carboxy-terminal region required by the adenovirus type 9 E4 ORF1 oncoprotein for transformation mediates direct binding to cellular polypeptides. J Virol 1997;71:7873–7880
50. Thomas DL, Schaack J, Vogel H, Javier R. Several E4 region functions influence mammary tumorigenesis by human adenovirus type 9. J Virol 2001;75: 557–568
51. Weiss RS, Gold MO, Vogel H, Javier RT. Mutant adenovirus type 9 E4 ORF1 genes define three protein regions required for transformation of CREF cells. J Virol 1997;71:4385–4394